Filtered backprojection method and the interior problem in 2D tomography

Anne Bilgot

TIMC-IMAG, UMR 5525, Université de Grenoble,
In3S, Faculté de Médecine, 38706 La Tronche, France

E-mail: Anne.Bilgot@imag.fr

Laurent Desbat

TIMC-IMAG, UMR 5525, Université de Grenoble,
In3S, Faculté de Médecine, 38706 La Tronche, France

E-mail: Laurent.Desbat@imag.fr

Valérie Perrier

Laboratoire Jean Kuntzmann, Université de Grenoble,
B.P. 53, 38401 Grenoble cedex 9, France

E-mail: Valerie.Perrier@imag.fr

Abstract. We address here the interior problem in local tomography, by means of filtered backprojection (FBP). This algorithm, traditionally used in the context of complete data, is usually not considered as valuable for the interior problem. However, in this article, we prove that as well as more sophisticated methods, the FBP algorithm ensures that the difference between the original and the reconstructed functions is continuous. We verify numerically that the FBP method can supply satisfactory images of discontinuities (on Shepp and Logan phantom and real data). Nevertheless, we also show limits of FBP, by pointing up examples on which the dependence on exterior structures damages the reconstruction quality in the Region Of Interest.

Keywords: Tomography, Filtered backprojection (FBP), local data, interior problem.
Submitted to: *Phys. Med. Biol.*

The interior problem, also known as the interior Radon transform inversion, is a particular case of 2D local tomography: it refers to the situation where only truncated data, and more precisely only X-Ray projections through a central section of a larger one, are available. It is known that the densities in this central section cannot be recovered, but that the discontinuities, *in some sense*, are. Thus, surfaces of discontinuity between anatomical structures are theoretically accessible [12, 11, 9, 15].

This problem occurs in particular in interventional reconstruction of tomographic sections: indeed, in the operating room, conventional CT-scanners can be used, but this technique is too expensive for a widespread use, and not satisfactory as regards ergonomy and irradiation of surgeon's hands. A promising alternative consists in *fluoroscopy-based reconstruction*, for which 2D X-Ray projection data are acquired using a C-Arm; this X-Ray imaging device is conventional in the operating room and much more ergonomic than a CT scanner [5, 7]; furthermore, it can nowadays be fitted with a digital, and so distortion-free, X-Ray detector. A drawback of this approach lies in the size of the detectors that can be manufactured today: they are likely to be not wide enough to collect the whole beam emerging from a section of a patient lying at the isocenter of the C-Arm. This lack of data prevents from applying conventional CT-reconstruction techniques, and the fact is that existing fluoroscopy-based reconstruction devices only enable to handle *exactly* small section structures, such as wrists or ankles [10]; this motivates the search for *local* algorithms, that is to say algorithms which are able to take the most of local data, so as to ensure, at least, that location of discontinuities is properly reconstructed.

Filtered backprojection method is the conventional inversion algorithm in case of global data. In case of local data, it is usually not considered as a valuable method, for it relies on the ramp filter: this filter is not compactly-supported and thus requires the knowledge of all projections. However, it is also usually known that in practice FBP method supplies satisfactory images of discontinuities. The goal of this paper is to assess efficiency of this algorithm as regards this point, and to tackle the following question: is FBP algorithm a relevant method for the interior problem? Our first answer is *yes*. Indeed, in section 2 we prove that, as well as more sophisticated methods, FBP algorithm ensures that the difference between the original and the reconstructed functions is a continuous function. In section 3 we illustrate this result on some images (phantom and real data). Nevertheless, in a second step, we point up examples which show that this method has also limits, as its dependence on exterior structures remains strong.

1. Introduction and Notations

1.1. Filtered Backprojection Method

Let first introduce some notations and classical formulas: let $\mathbf{S}^1$ denotes the unit circle in $\mathbf{R}^2$; the Radon Transform of $f \in \mathbf{L}^1(\mathbf{R}^2)$ is defined by

$$\forall(\mathbf{\Theta}, s) \in \mathbf{S}^1 \times \mathbf{R},\ \mathcal{R}_\theta f(s) \stackrel{\text{def}}{=} \mathcal{R}f(\mathbf{\Theta}, s) \stackrel{\text{def}}{=} \int_{\{\mathbf{x}\in\mathbf{R}^2 | \mathbf{x}\cdot\mathbf{\Theta}=s\}} f(\mathbf{x}) d\mathbf{x}$$

where "$\cdot$" is the euclidean inner product, $\theta \in [0, 2\pi[$, $\Theta = (\cos\theta, \sin\theta)$. The Radon transform is known to be invertible through the Fourier domain, using the projection-slice theorem which states that, for $\omega \in \mathbf{R}$,

$$\widehat{\mathcal{R}_\theta f}(\omega) = \sqrt{2\pi}\widehat{f}(\omega\mathbf{\Theta})$$

where for all $n \in \mathbf{N}^*$, the Fourier Transform of $f \in \mathbf{L}^1(\mathbf{R}^n)$ is normalized in the following way: for $\mathbf{k} \in \mathbf{R}^n$,

$$\hat{f}(\mathbf{k}) = \frac{1}{\sqrt{2\pi}^n} \int_{\mathbf{R}^n} f(\mathbf{x}) e^{-i\mathbf{x}\cdot\mathbf{k}} d\mathbf{k}$$

This leads to the well-known filtered backprojection inversion formula [11]:

$$f(\mathbf{x}) = \frac{1}{\sqrt{2\pi}^3} \int_0^\pi \int_{\mathbf{R}} \widehat{\mathcal{R}_\theta f}(\omega) |\omega| e^{i\omega \mathbf{x}\cdot\mathbf{\Theta}} d\omega d\theta$$

which can be reformulated as [11]:

$$f(\mathbf{x}) = \frac{1}{4\pi^2} \int_0^{2\pi} \left(\mathrm{vp}\left(\frac{1}{x}\right) * \partial_s \mathcal{R}_\theta f \right)(\mathbf{x}\cdot\mathbf{\Theta})\, d\theta = \frac{1}{4\pi^2} \int_0^{2\pi} \left(\lim_{\epsilon \to 0^+} \int_{u\in\mathbf{R};|\mathbf{x}\cdot\mathbf{\Theta}-u|>\epsilon} \frac{\partial_s \mathcal{R}_\theta f(u)}{\mathbf{x}\cdot\mathbf{\Theta} - u} du \right) d\theta$$

1.2. The interior problem

Let a $(0 < a < 1)$ be the radius of the Region Of Interest (ROI), which, here, is assumed to be also the region of exposure. The interior problem is defined as follows: using only the interior components of the Radon transform,

$$(\mathcal{R}f)_{\mathrm{int}} = \left\{ \mathcal{R}f(\mathbf{\Theta}, s); \mathbf{\Theta} \in \mathbf{S}^1, s \in [-a, a] \right\}$$

is it possible to reconstruct the values of f inside the ROI? The response is well known (see for instance [11]): it is not possible, and more precisely, the interior problem is ill-posed in the sense that it is not uniquely solvable. Let us suppose that we apply the inverse of the Radon transform $\mathcal{R}^{-1}$ to the interior data only, in order to estimate f in the ROI. The set of non-considered data in the interior problem will be denoted by:

$$(\mathcal{R}f)_{\mathrm{ext}} \stackrel{\mathrm{def}}{=} \left\{ \mathcal{R}f(\mathbf{\Theta}, s); \mathbf{\Theta} \in \mathbf{S}^1, |s| > a \right\}.$$

As illustrated in Fig 1:

- left: when a structure with support included in the ROI is considered, the Radon transform has only interior components $(\mathcal{R}f = (\mathcal{R}f)_{\mathrm{int}})$;
- right: when a structure with support outside the ROI is considered, the Radon transform has exterior components $((\mathcal{R}f)_{\mathrm{ext}})$, *but also* interior components $((\mathcal{R}f)_{\mathrm{int}} \neq \mathbf{0})$.

Therefore, when a function $f = f_{\mathrm{int\_2D}} + f_{\mathrm{ext\_2D}}$ with structures both in the ROI $(f_{\mathrm{int\_2D}})$ and outside the ROI $(f_{\mathrm{ext\_2D}})$ is dealt with, the available data in the interior problem are made of two components:

$$(\mathcal{R}f)_{\mathrm{int}} = \mathcal{R}f_{\mathrm{int\_2D}} + (\mathcal{R}f_{\mathrm{ext\_2D}})_{\mathrm{int}}$$

and the inversion of these data using global inversion operator, denoted here by $\mathcal{R}^{-1}$, leads to the reconstruction of the following function:

$$f_{\mathrm{loc}} = \mathcal{R}^{-1}\left((\mathcal{R}f)_{\mathrm{int}}\right) = \mathcal{R}^{-1}\left(\mathcal{R}f_{\mathrm{int\_2D}}\right) + \mathcal{R}^{-1}\left((\mathcal{R}f_{\mathrm{ext\_2D}})_{\mathrm{int}}\right) = f_{\mathrm{int\_2D}} + \mathcal{R}^{-1}\left((\mathcal{R}f_{\mathrm{ext\_2D}})_{\mathrm{int}}\right)$$

Thus, in the ROI, the initial function $f_{\text{int\_2D}}$ is corrupted by $\mathcal{R}^{-1}\left(\left(\mathcal{R}f_{\text{ext\_2D}}\right)_{\text{int}}\right)$ which generally does not cancel in the ROI in 2D. This bias is present in all even dimensions and observable in reconstructions. This bias usually motivates the search for other reconstruction methods, such as local methods.

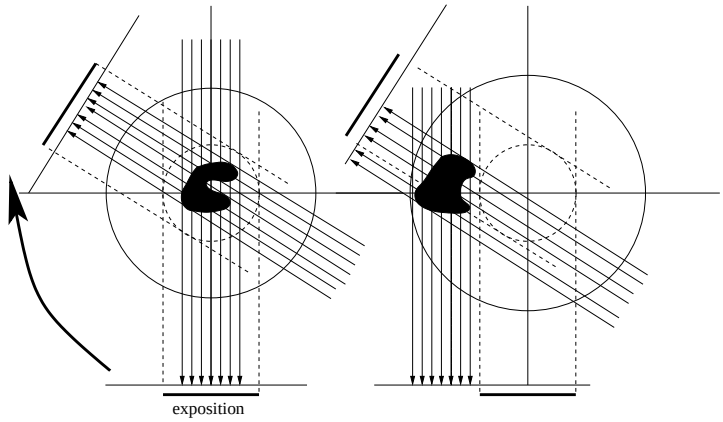

Figure 1. Interior problem in 2D parallel geometry: on the left, the object is entirely included in the ROI (dashed circle): the Radon transform reduces to interior data. On the right, the object lies in the exterior of the ROI: the Radon transform data have not only exterior contributions, but also interior contributions.

1.3. Local methods for the interior problem

1.3.1. The purpose of these methods The purpose of local methods dedicated to the interior problem is usually the following: they aim at "reconstructing discontinuities" in the ROI (in the sense: to reconstruct a function with discontinuities exactly located as in the initial function, or, sometimes, even with the same jumps).
The legitimacy of such a purpose relies on a theorem of micro-local analysis, established by Quinto [12]: this theorem links the singular supports (which correspond to discontinuity curves) and more precisely the wavefronts (which additionally give the normal directions) of f and $\mathcal{R}f$ (see [12] for details):

Theorem 1.1 (Wavefront conservation [12])
- *If* $(\mathbf{x_0}, \mathbf{\Theta_0}) \in \mathbf{R}^2 \times \mathbf{S}^1$ *belongs to the wavefront of* f*, then the point* $(\mathbf{\Theta_0}, \mathbf{\Theta_0} \cdot \mathbf{x_0})$ *of the sinogram belongs to the singular support of* $\mathcal{R}f$*, with associated normal vector* $(-\mathbf{x_0} \cdot \mathbf{\Theta_0}^{\perp}, 1)$ *(*$\mathbf{\Theta_0}^{\perp}$ *denoting the direct orthogonal vector to* $\mathbf{\Theta_0}$*): this means that* $\left((\mathbf{\Theta_0}, \mathbf{\Theta_0} \cdot \mathbf{x_0}), (-\mathbf{x_0} \cdot \mathbf{\Theta_0}^{\perp}, 1)\right)$ *belongs to the wavefront of* $\mathcal{R}f$*.*
- *Conversely, if* $(\mathbf{\Theta_0}, s_0) \in \mathbf{S}^1 \times \mathbf{R}$ *belongs to the singular support of* $\mathcal{R}f$*, and if at this point the tangent to the singular support is directed by the vector* $(1, p)$ *(where* $p \in \mathbf{R}$*), then, in the direct domain* $\mathbf{R}^2$*, the point* $s_0\mathbf{\Theta_0} + p\mathbf{\Theta_0}^{\perp}$ *belongs to the singular support of* f *and* $(s_0\mathbf{\Theta_0} + p\mathbf{\Theta_0}^{\perp}, \mathbf{\Theta_0})$ *belongs to the wavefront of* f*.*

Thus, the discontinuity curves of f can be recovered from the discontinuity curves of $\mathcal{R}f$. This is the strategy proposed in geometrical approaches [13, 15], but, actually, the

detection of discontinuities within a sinogram is not an easy task: an insight is given on figure 2 with the example of a simple phantom given on the left, for which the singular support of its sinogram, on the right, has a complex structure (this singular support can be computed using theorem (1.1) and parametrized representations of the singular supports in both domains - see [3] for details); geometrical methods [13, 15], which consist in detecting discontinuities in the sinogram before deducing the discontinuities in the image, are thus not easy to implement.

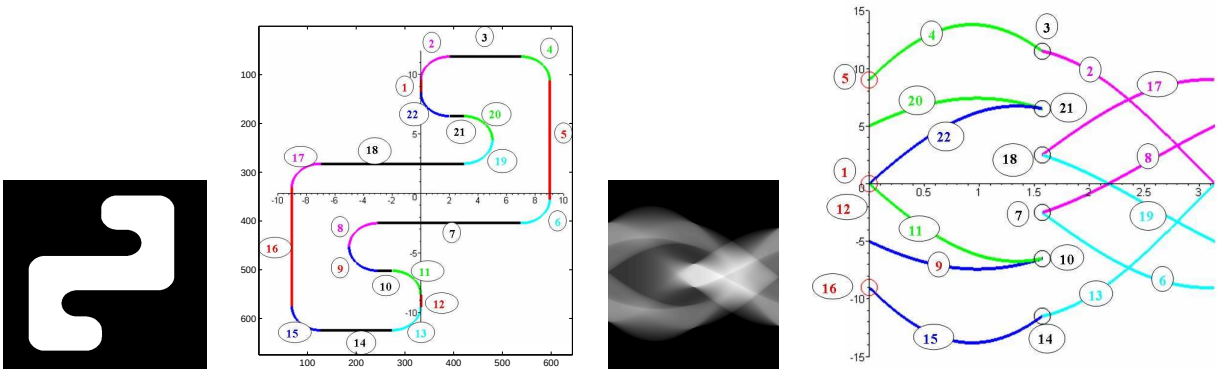

Figure 2. Correspondence between the singular support of f (images on the left) and the singular support of its Radon transform (on the right) (the correspondence is materialized by corresponding numbers): f has a simple support, and, nevertheless, the singular support of its Radon transform is rather complicated.

1.3.2. State of the art The literature provides several approaches to the interior problem:

- Λ-*Tomography* (see for instance [6]) where one reconstructs Λf instead of f (the pseudo-differential operator Λ, defined by $\widehat{\Lambda f}(\mathbf{k}) = |\mathbf{k}|\hat{f}(\mathbf{k})$, is locally recoverable, and known to preserve the discontinuities);
- *Pseudolocal Tomography* [9], where one copes with the non-locality of the ramp filter by truncating it in the direct domain. We detail this method below.
- Wavelet based-methods where separable [14, 2] or non separable [4] multiresolution analysis are recovered using local data: the 2D wavelet transform of a function f can be computed from a 1D wavelet transform of its Radon transform $\mathcal{R}f$; it can be seen as a generalization of the FBP algorithm. The locality of the wavelet filtering enables to reconstruct wavelet coefficients of the function f *up to a given scale* (according to the range of availability of data) (fine details, and therefore discontinuities, are thus visible). A generalization of wavelet based-methods, relying on theoretical work by Holschneider [8], is also applied to the interior problem in [3].

In the following, we show that the classical FBP method is also relevant in this context.

2. Truncated formulas for truncated data

In the following we introduce the *Truncated Filtered Backprojection* method: this is filtered backprojection applied to interior data. Whereas in pseudo-local tomography the same filter of constant width is applied to all projections (truncated data are over-truncated to fit with the filter width), in Truncated Filtered Backprojection the *filtering* operator is no more a filter (it is shift-variant), and all the available data are used.

From now, we suppose that f is compactly supported in the open unit disk of $\mathbf{R}^2$.

2.1. Pseudo-local tomography

This method has been designed by A. Katsevitch and A. Ramm [9]. The idea consists in truncating the ramp filter in the direct domain so as to filter local data with a filter restricted to an interval $[-d, d]$ (where $d > 0$ and for treatment of local data $d << a$); thus, instead of reconstructing f with formula

$$f(\mathbf{x}) = \frac{1}{4\pi^2} \int_0^{2\pi} \left(\lim_{\epsilon \to 0^+} \int_{s \in \mathbf{R}; |\mathbf{x}\cdot\mathbf{\Theta} - s| > \epsilon} \frac{\partial_s \mathcal{R}_\theta f(s)}{\mathbf{x}\cdot\mathbf{\Theta} - s} ds \right) d\theta$$

one reconstructs the function f_d, defined by:

$$f_d(\mathbf{x}) = \frac{1}{4\pi^2} \int_0^{2\pi} \left(\lim_{\epsilon \to 0^+} \int_{\epsilon < |\mathbf{x}\cdot\mathbf{\Theta} - s| < d} \frac{\partial_s \mathcal{R}_\theta f(s)}{\mathbf{x}\cdot\mathbf{\Theta} - s} ds \right) d\theta$$

The reconstruction of f_d can be made locally, in the sense that the reconstruction of f at point $\mathbf{x}$ only requires the knowledge of $\mathcal{R}f$ across the disk of center $\mathbf{x}$ and radius d. To identify the information on f present in f_d, the authors introduce the function f_d^C, difference between f_d and the reference function f, defined by:

$$f_d^C(\mathbf{x}) = f(\mathbf{x}) - f_d(\mathbf{x})$$

The key theorem of pseudo-local tomography for the interior problem is the following:

Theorem 2.1 (Discontinuities and pseudo-local tomography [9]) *For all $d > 0$, the function f_d^C is continuous in the direct domain.*

The interpretation of this property then follows: for all $d > 0$, f_d holds discontinuities of f, that is to say the discontinuities of f_d are exactly the same as those of f (location as well as amplitude). The proof of this result is based on continuity properties of integrals with parameters, and can be found in [9].

In this approach the filtering steps do not use all the range of data that are available in $(\mathcal{R}f)_{\text{int}}$ (the filter is the same wherever it is applied).

2.2. Truncated FBP

In the context of Truncated FBP, we introduce the following reconstructed function:

$$f^a_{\mathrm{TFBP}}(\mathbf{x}) = \frac{1}{4\pi^2}\int_0^{2\pi} \Lambda^a_{\mathrm{TFBP}}\mathcal{R}_\theta f(\mathbf{x}\cdot\mathbf{\Theta})d\theta$$

where

$$\Lambda^a_{\mathrm{TFBP}}\mathcal{R}_\theta f(s) = \lim_{\epsilon\to 0^+}\left[\int_{-a}^{s-\epsilon}\frac{\partial_s\mathcal{R}_\theta f(u)}{s-u}du + \int_{s+\epsilon}^{a}\frac{\partial_s\mathcal{R}_\theta f(u)}{s-u}du\right]$$

In contrast with pseudo-local tomography,

(i) all the data that are available are used;

(ii) the "filtering" operator applied to the data depends on the point where it is applied: the ramp filter is truncated in the direct domain to the interval $[s-a, s+a]$, *depending on* s. Therefore, *stricto sensu*, we do not apply a filter any more (the operator is not invariant by translation).

The question that should be addressed now is: what can be learnt about f according to f^a_{TFBP}?
In [11], Natterer gives an answer to a very close question: in the context of C^∞-functions, he proposes to complete the interior data Rf by consistency into the whole domain. Applying the FBP to these completed data, he proves that the reconstructed function only differs from the original one up to an essentially constant function.

Giving an another point of view, we introduce the difference between the original function f and f^a_{TFBP}:

$$\left(f^a_{\mathrm{TFBP}}\right)^C(\mathbf{x}) = \frac{1}{4\pi^2}\int_0^{2\pi}\left[\int_{-1}^{-a}\frac{\partial_s\mathcal{R}_\theta f(s)}{\mathbf{x}\cdot\mathbf{\Theta}-s}ds + \int_a^1\frac{\partial_s\mathcal{R}_\theta f(s)}{\mathbf{x}\cdot\mathbf{\Theta}-s}ds\right]d\theta \qquad (1)$$

and we will prove in the following that $\left(f^a_{\mathrm{TFBP}}\right)^C$ is a continuous function in the ROI, as in pseudo-local tomography. Therefore the discontinuities of f^a_{TFBP} are exactly the same as the discontinuities of f within the ROI.

Theorem 2.2 (Discontinuities and Truncated Filtered Backprojection) *For all $a>0$, the function $\left(f^a_{\mathrm{TFBP}}\right)^C$ is continuous in the disk $\{\mathbf{x}\in\mathbf{R}^2; |\mathbf{x}|\le r\}$, for all r such that $0<r<a$.*

Proof: By an integration by parts on (1) (we recall that $\mathcal{R}_\theta f(-1) = \mathcal{R}_\theta f(1) = 0$ for all θ):

$$\left(f^a_{\mathrm{TFBP}}\right)^C(x) = \frac{1}{4\pi^2}\int_0^{2\pi}\left(\left[\frac{\mathcal{R}_\theta f(s)}{\mathbf{x}\cdot\mathbf{\Theta}-s}\right]_{-1}^{-a} + \int_{-1}^{-a}\frac{\mathcal{R}_\theta f(s)}{(\mathbf{x}\cdot\mathbf{\Theta}-s)^2}ds + \left[\frac{\mathcal{R}_\theta f(s)}{\mathbf{x}\cdot\mathbf{\Theta}-s}\right]_a^1 + \int_a^1\frac{\mathcal{R}_\theta f(s)}{(\mathbf{x}\cdot\mathbf{\Theta}-s)^2}ds\right)d\theta$$

$$= \frac{1}{4\pi^2}\int_0^{2\pi}\left(\frac{\mathcal{R}_\theta f(-a)}{\mathbf{x}\cdot\mathbf{\Theta}+a} - \frac{\mathcal{R}_\theta f(a)}{\mathbf{x}\cdot\mathbf{\Theta}-a}\right)d\theta \qquad (2)$$
$$+ \frac{1}{4\pi^2}\int_0^{2\pi}\left(\int_{-1}^{-a}\frac{\mathcal{R}_\theta f(s)}{(\mathbf{x}\cdot\mathbf{\Theta}-s)^2}ds + \int_a^1 \frac{\mathcal{R}_\theta f(s)}{(\mathbf{x}\cdot\mathbf{\Theta}-s)^2}ds\right)d\theta$$

Let us now consider the closed disk D_r, of radius r, strictly included in the region of exposure (*ie* $r < a$), and a point $\mathbf{x}$ within D_r. In the following, we check that the conditions that are required to apply the results about continuity of integrals with parameters are fulfilled, so as to prove that $(f^a_{\mathrm{TFBP}})^C$ is continuous at point $\mathbf{x}$.
For the first integral in (2), we have:

- for all $\theta \in [0, 2\pi[$, the functions $\mathbf{x} \mapsto \dfrac{\mathcal{R}_\theta f(-a)}{\mathbf{x}\cdot\mathbf{\Theta}+a}$ and $\mathbf{x} \mapsto \dfrac{\mathcal{R}_\theta f(a)}{\mathbf{x}\cdot\mathbf{\Theta}-a}$ are continuous in D_r (because for each θ, $\mathbf{x}\cdot\mathbf{\Theta} \pm a$ never vanishes, as $|\mathbf{x}\cdot\mathbf{\Theta}| \leq |\mathbf{x}| \leq r < a$);

- moreover for all $\mathbf{x} \in D_r$, $-r < \mathbf{x}\cdot\mathbf{\Theta} < r$, we have $0 < a - r < \mathbf{x}\cdot\mathbf{\Theta} + a$, and then

  $$\left|\frac{\mathcal{R}_\theta f(-a)}{\mathbf{x}\cdot\mathbf{\Theta}+a}\right| \leq \frac{|\mathcal{R}_\theta f(-a)|}{a-r}$$

  which is a function (of θ), integrable on $[0, 2\pi]$.

  A similar argument can be used for the function $\mathbf{x} \mapsto \dfrac{\mathcal{R}_\theta f(a)}{\mathbf{x}\cdot\mathbf{\Theta}-a}$; it follows that the first integral of (2) is a continuous function of $\mathbf{x}$ in D_r.

For the second integral in (2), we have:

- for each couple $(\theta, s) \in [0, 2\pi[\times[-1, -a]$ (resp. each couple $(\theta, s) \in [0, 2\pi[\times[a, 1]$), the function $\mathbf{x} \mapsto \dfrac{\mathcal{R}_\theta f(s)}{(\mathbf{x}\cdot\mathbf{\Theta}-s)^2}$ is continuous in D_r (because $\mathbf{x}\cdot\mathbf{\Theta} - s$ never vanishes);

- moreover for all $\mathbf{x} \in D_r$, for all $(\theta, s) \in [0, 2\pi[\times[-1, -a]$,

  $$0 < -r + a \leq -r - s \leq \mathbf{x}\cdot\mathbf{\Theta} - s$$

  therefore

  $$\left|\frac{\mathcal{R}_\theta f(s)}{(\mathbf{x}\cdot\mathbf{\Theta}-s)^2}\right| \leq \left|\frac{\mathcal{R}_\theta f(s)}{(a-r)^2}\right|$$

  the r.h.s. being a function of (θ, s), integrable on $[0, 2\pi[\times[-1, -a]$.

A similar proof can be made for the third integral of (2): the sum of the second and the third integral is thus a continuous function of $\mathbf{x}$ in D_r. ■

3. Discussion and tests

3.1. First experiments

Example 1: Shepp and Logan phantom We first show reconstruction results obtained by Truncated Filtered Backprojection applied to Shepp and Logan phantom

(displayed on the first line of figure 3, with a zoom-in on the ROI displayed on the right).
We fix $a > 0$ and simulate the truncated Radon transform of the phantom:

$$\forall(\mathbf{\Theta}, s) \in \mathbf{S}^1 \times [-1, 1],\ g(\mathbf{\Theta}, s) = \begin{cases} \mathcal{R}f(\Theta, s) \text{ if } |s| \leq a \\ 0 \text{ else} \end{cases} \tag{3}$$

The results are displayed on the left of figure 3 (second and third line). The initial image is the square $[-1, 1]^2$ sampled on 256^2 pixels. The radius of the ROI is $a = 0.25$, and the data are acquired on 450 equiangular projections on $[0, \pi[$, each of them sampled with a step $\frac{2}{256}$.

There is only a bias, roughly constant in the ROI, between the phantom and the reconstruction, and as Theorem 2.2 asserts, the discontinuities of the phantom are clearly visible in the reconstruction. Although this reconstruction is satisfactory if one aims at localizing discontinuities, it is common in local tomography literature to use a procedure to reduce artefacts at the ROI boundary [14, 4]: it consists in erasing discontinuities at the truncated sinogram boundary, by extending by continuity interior data in a constant way:

$$\forall(\Theta, s) \in \mathbf{S}^1 \times [-1, 1],\ g(\mathbf{\Theta}, s) = \begin{cases} \mathcal{R}f(\mathbf{\Theta}, s) \text{ if } |s| \leq a \\ \mathcal{R}f(\mathbf{\Theta}, a) \text{ if } s > a \\ \mathcal{R}f(\mathbf{\Theta}, -a) \text{ if } s < -a \end{cases} \tag{4}$$

Theorem 2.2 is still valid: discontinuities of the reconstruction are the same than the ones of the phantom. The results are displayed on the right of figure 3 (second and third line). The artefacts in the reconstruction are clearly reduced at the borders at the ROI boundary, as well as the amplitude of the bias in the ROI. Discontinuities are still clearly visible, but the visual similarity (as regards gray levels) with the phantom is much improved: local reconstruction really "looks like" the phantom.

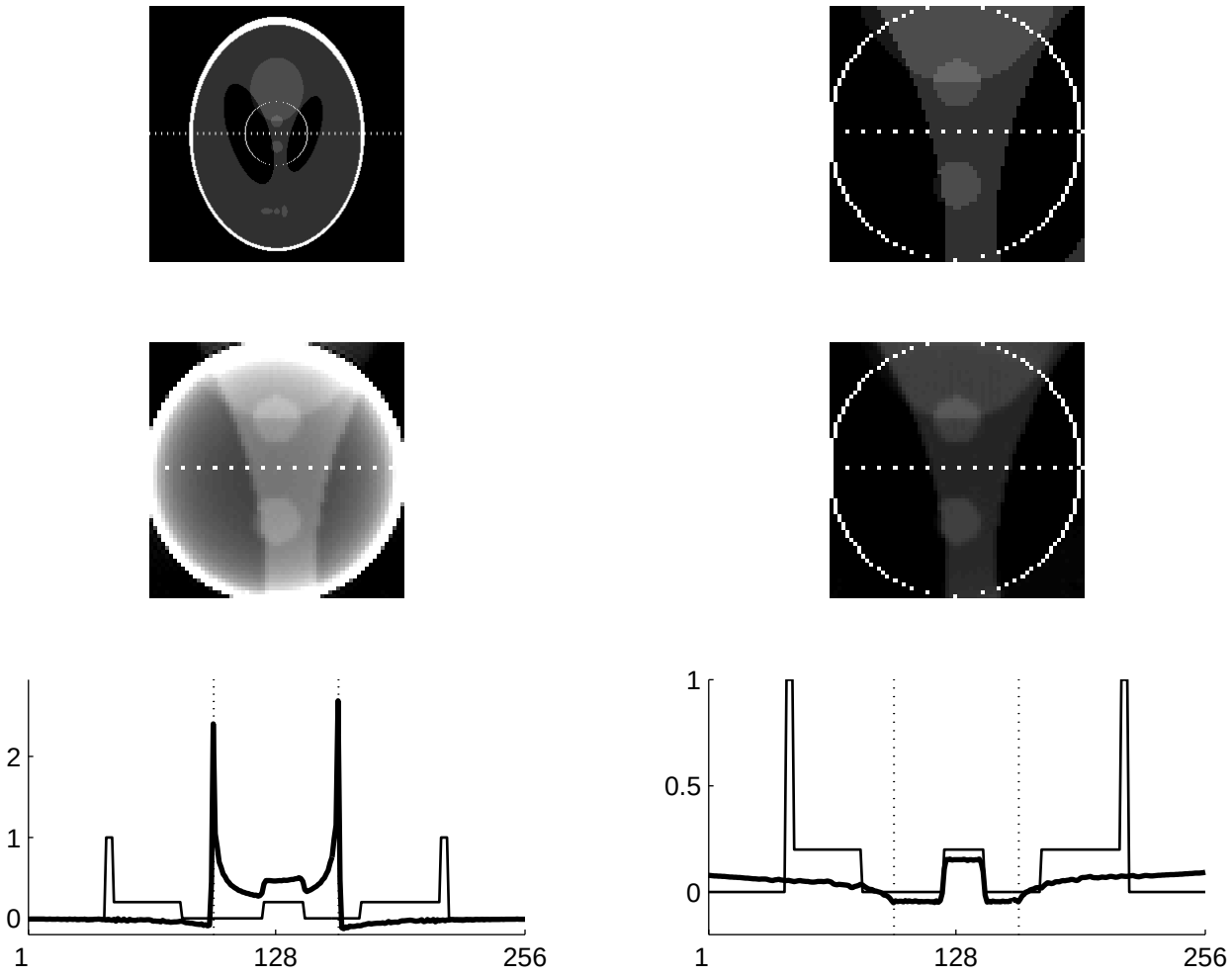

Figure 3. Results of TFBP applied on interior data on Shepp and Logan phantom. First line, the phantom, with, on the right, a zoom-in on the ROI. Second and third line, on the left: reconstructions from *raw* local data (exterior data are zero), and on the right, reconstructions from data extended by continuity. Third line, in both cases, a zoom-in on the ROI of the reconstruction and comparisons between the phantom and the reconstruction horizontal cross-sections are displayed (the darker line stands for the reconstruction). Note that the values of the jumps are well estimated.

Example 2: Real data

We have then applied TFBP technique on real data (human trabecular bone sample), kindly provided by F. Peyrin [1], and acquired on the medical line of ESRF Grenoble (European Synchrotron Radiation Facility). The projections were sampled on 1024 pixels of 15 μm, for 900 directions. The length of the medical line is 145 m, thus we consider that parallel beam conditions are fulfilled. Results are displayed on figure 4. They are fully satisfactory: even small details in the ROI are well localized in the reconstruction.

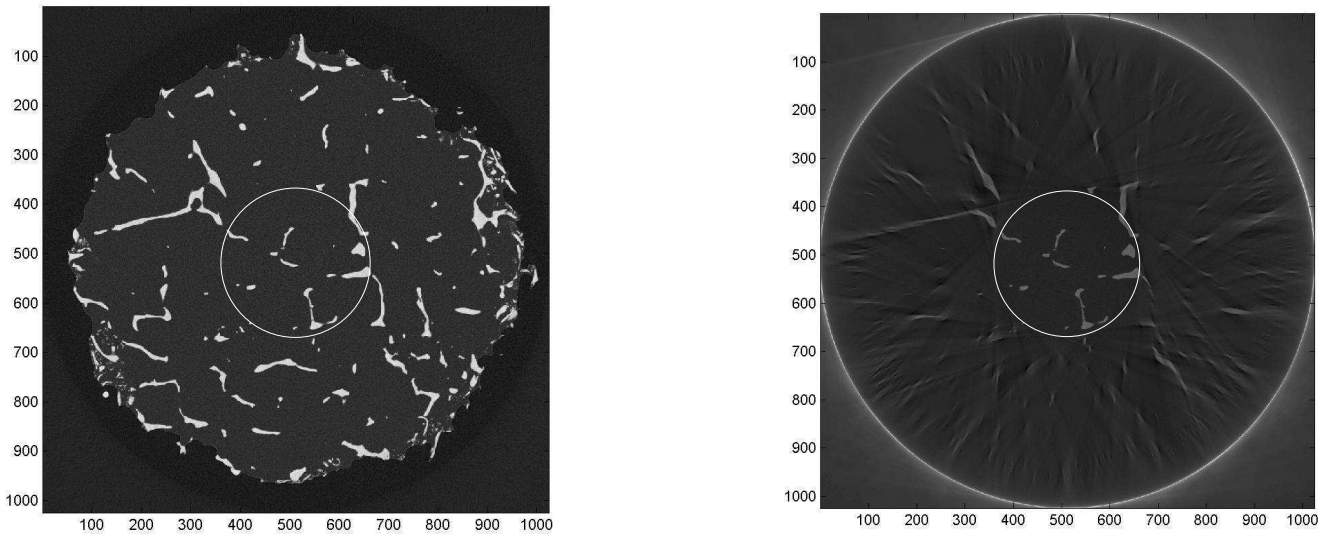

Figure 4. FBP-reconstruction results on real data (human trabecular bone sample data, kindly provided by F. Peyrin, ESRF Grenoble [1]). These data were acquired at ESRF (European Synchrotron Radiation Facility) on the medical line. The projections were sampled on 1024 pixels of 15 μm, for 900 directions. The similarity between the reconstruction from global data (left) and local data (right) is fully satisfactory in the ROI, even for small details.

3.2. Some limits

Both previous examples tend to show that TFBP is a very satisfactory method for the interior problem. In order to assess the range of efficiency of TFBP, we have tried to build phantoms for which TBFP behaviour is less convincing. As explained in paragraph 1.2, the bias created in the ROI in case of local data comes from exterior structures: we have thus tried to compare influences of several kinds of exterior structures, by designing phantoms where only exterior structures are present. Results are displayed in figure 5 (interior data have been extended by continuity).

It thus appears that in case of Shepp and Logan phantom, the different contributions of external data tend to compensate in the ROI, thus creating a bias which is roughly constant, and thus leading to visually very satisfactory local reconstruction results. On the contrary, for the second and the third phantoms, we have put structures with high density, non-symmetrically distributed around the ROI. The bias implied in the ROI has no discontinuity (as theory proves), but has significant decay in the ROI (with even an inflection point in the third case). Therefore, the identification of discontinuities in the ROI is not compromised, but dissymmetry is forced in the ROI. Consequently, in case of such exterior structures, two similar structures in the ROI can be reconstructed in two different ways. Such an example is given in figure 6: disks are not reconstructed with the same gray levels whether they are close to the white exterior rectangles or not. In such a case, the reconstruction image tends to show that the two structures have

different densities, whereas they actually have the same.

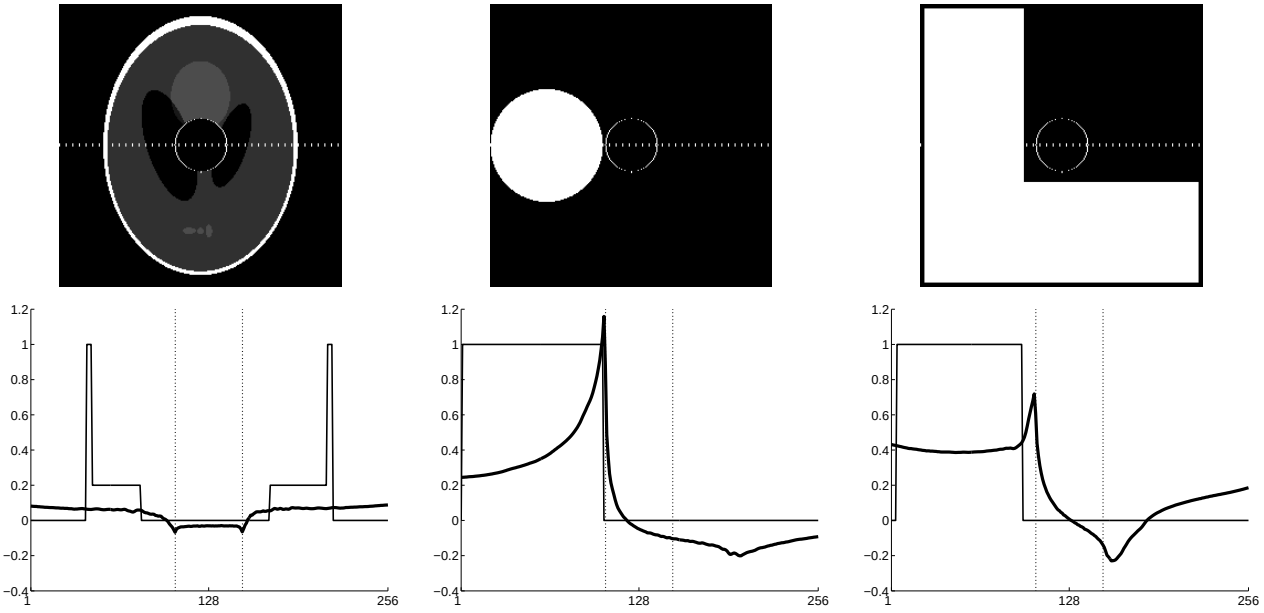

Figure 5. Comparisons of the influence of three kinds of exterior data on the TFBP-reconstruction within the ROI. The three phantoms are displayed on the first line, and the reconstructions obtained by TFBP applied on interior data are displayed on the second one. For the Shepp and Logan phantom (left), only a constant bias is created. In the two other cases, with high density exterior structures localized only on some sides of the ROI, the bias has significant decay across the ROI: a dissymmetry is thus created in the ROI.

3.3. Comparison with other local methods

- The main advantage of TFBP in comparison with other local methods is its simplicity: conventional FBP algorithm, easily available, can be used without any modification.
- Thanks to the theoretical result stated in this paper, TFBP, like Λ-tomography and pseudo-local tomography, provides a reconstructed function which has the same discontinuities as the reference function.
- TFBP has exactly the same complexity as FBP; it is well-known that the most expensive step is the backprojection, present in all considered local methods. Therefore, the complexity argument is not very significative.
- Finally, the main drawback of TFBP is its still unpredictable "qualitative performance", due to its might-be dependence on exterior structures. For a given function f, other local algorithms, which implement truly local filters, reconstruct in the ROI the same function whether the sinogram is complete or not; it is not the case for TFBP.

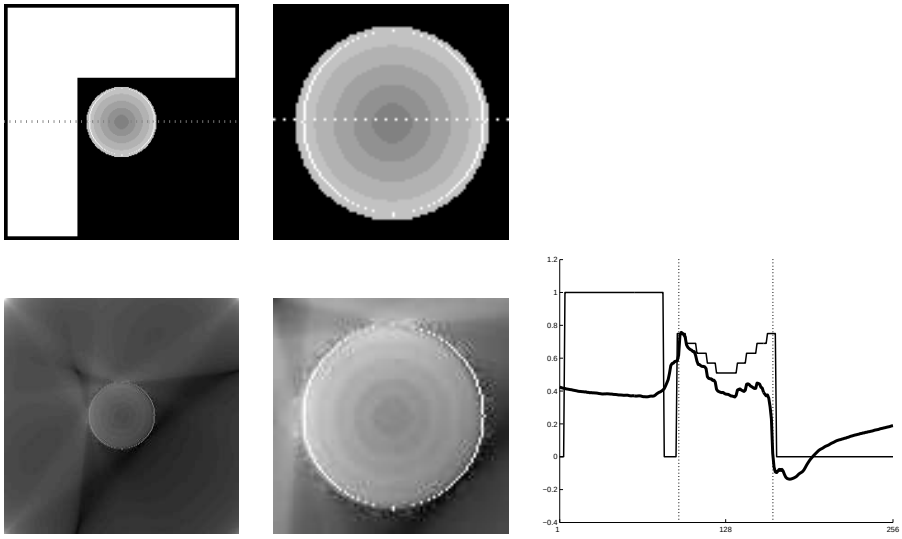

Figure 6. Example where exterior data have influence on the TFBP-reconstruction in the ROI. The phantom is displayed on the first line, with a zoom-in on the ROI, the reconstruction obtained by TFBP on the second line, and the comparison of cross-sections on the third line. A significant dissymmetry is created in the ROI by TFBP.

4. Conclusion

In this paper we have studied the behavior of "Truncated Filtered Backprojection" (that is to say FBP applied on interior problem data). As for pseudo-local tomography, we have proved that the difference between the reference function and the reconstructed function is continuous on the ROI. This supplies a justification to an experimental intuition: this simple method provides with very satisfactory results if one is only interested in the location of discontinuities in the reconstruction. Furthermore, we have shown that on some examples, such as the well-known Shepp and Logan phantom, this method goes further: the visual similarity between the two images can be very high. Nevertheless, we have also shown that this is not true for all images: TFBP method remains strongly dependent on exterior structures. As shown on an example, this similarity can be significantly damaged. In conclusion, if not only discontinuities but also symmetry preservation is crucial in the application, other local methods should be considered. If only discontinuity localization is sufficient, the TFBP algorithm is a very simple and efficient method.

Acknowledgments

The authors would like to acknowledge Françoise Peyrin for fruitful discussions and for providing the ESRF data presented in figure 4.

References

[1] Apostol L., Boudousq V., Basset O., Odet C., Yot S., Tabary J., Dinten J M., Boller E., Kotzki P O., Peyrin F., *Relevance of 2D radiographic texture analysis for the assessment of 3D bone micro-architecture*, Med Phys, vol. 33(9), pp. 3546-3556, 2006.

[2] Berenstein, C. and Walnut, D. *Wavelets and Local Tomography*, in *Wavelets in Medicine and Biology*, CRC Press, Aldroubi and Unser eds, pp. 231-261, 1996.

[3] Bilgot, A. *Méthodes locales d'identification de surfaces de discontinuité à partir de projections tronquées pour l'imagerie interventionnelle.* PhD Thesis Université J. Fourier, Grenoble I, 2007.

[4] Bonnet, S. and Peyrin, F. and Turjman, F. and Prost, R. *Tomographic reconstruction using nonseparable wavelets*, IEEE Transactions on image processing, vol.9(8), pp. 1445-1450, 2000.

[5] Euler, E. and Heining, S. and Riquarts, C. and Mutschler, W. *C-Arm-based three-dimensional navigation: a preliminary feasibility study* Computer Aided Surgery, vol. 8(1), pp. 35-41, 2003.

[6] Faridani, A. and Buglione, K.A. and Huabsomboon, P. and Iancu, O.D. and McGrath, J. *Introduction to Local Tomography*, in *Radon Transforms and Tomography*, American Mathematical Society, Contemporary Mathematics, vol. 278, pp. 29-47, 2001.

[7] Fleute, M. and Lavallée, S. and Desbat, L., *Integrated Approach for Matching Statistical Shape Models with Intra-operative 2D and 3D Data.*, in *Proceedings of MICCAI*, Dohi, T. and Kikinis, R. eds., Springer-Verlag, 2002.

[8] Holschneider, M. *Inverse Radon transforms through inverse wavelet transforms*, Inverse Problems vol.7, pp. 853-861, 1991.

[9] Katsevich, A.I. and Ramm, A.G. *Pseudolocal Tomography*, SIAM Journal of Applied Mathematics, vol.56(1), pp. 167-191, 1996.

[10] Kendoff, D. and Citak, M. and Hüfner, T. and Chaudhary, S. and Krettek, C. *Current concepts and applications of computer navigation in orthopedic trauma surgery*, Central European Journal of Medicine, vol.2(4), pp. 392-403, 2007.

[11] Natterer, F. *The Mathematics of Computerized Tomography* , SIAM, Classics in Applied Mathematics, 2001.

[12] Quinto, E.T. *Singularities of the X-ray transform and limited data tomography in* $\mathbf{R}^2$ *and* $\mathbf{R}^3$, SIAM J. Math. Anal., vol.24, pp. 1215-1225, 1993.

[13] Ramm, A.G. and Katsevich, A.I. *The Radon Transform and Local Tomography*, CRC Press, 1996.

[14] Rashid Farrokhi, F. and Ray Liu, K.J. and Berenstein, C. and Walnut, D. *Wavelet-based multiresolution local tomography*, IEEE Transactions on Image Processing, vol.6(10), pp. 1412-1429, 1997.

[15] Thirion, J.-P., *Segmentation of tomographic data without image reconstruction*, IEEE Transactions on Medical Imaging, vol.11(1), pp. 102-110, 1992.